RSC Pharmaceutics

ROYAL SOCIETY OF CHEMISTRY

PAPER

View Article Online
View Journal

Cite this: DOI: 10.1039/d5pm00327j

Needle-free transdermal delivery of mRNA vaccine with ionic liquid crystals and effective tumor growth inhibition

Tomohiro Higashi,[a] Keisuke Tanaka,[a] Kiyohiro Toyofuku,[a] Rie Wakabayashi,[a,b] Yoshirou Kawaguchi,[a] Noriho Kamiya[a,b,c] and Masahiro Goto[*a,b,c]

mRNA vaccines have emerged as a promising therapeutic option based on their ability to elicit a strong immune response, the reduced risk of genomic integration, and the potential to produce various vaccine candidates using the same manufacturing process. However, current mRNA vaccines primarily rely on injection-based administration, which is an invasive procedure that requires a healthcare professional. To address these limitations, transdermal delivery has been proposed as a non-invasive alternative. However, the stratum corneum (SC) acts as a formidable barrier to biopharmaceuticals penetration, necessitating innovative approaches for effective transdermal vaccination. In this study, we developed a novel ionic liquid crystal (ILC), which was formulated from a lyotropic liquid crystal (LLC) using ionic liquids (ILs) with amphiphilic molecular properties. ILC formulations were prepared by mixing ILs with ultrapure water and demonstrated optimal viscoelastic properties for transdermal application. *In vitro* skin permeation assays revealed the superior mRNA penetration of ILC formulations compared with aqueous mRNA solutions. Furthermore, *in vivo* evaluation using a tumor-bearing mouse model revealed that transdermal mRNA delivery *via* ILCs significantly suppressed tumor growth and promoted CD8+ T-cell infiltration into tumor tissues, indicating a potent antitumor effect. These findings highlight the potential of ILC-based transdermal mRNA delivery as a promising strategy for the development of next-generation mRNA vaccine administration methods.

Received 10th November 2025,
Accepted 9th March 2026

DOI: 10.1039/d5pm00327j

rsc.li/RSCPharma

Introduction

The remarkable success of mRNA vaccines against SARS-CoV-2 has led to global interest in RNA-based therapeutics, including mRNA, siRNA, and miRNA. Among these, mRNA vaccines exhibit a fundamentally different mechanism of action from conventional pharmaceuticals, as they introduce synthetic mRNA into the body, allowing for intracellular expression of target proteins to exert therapeutic effects. This mechanism allows for the tailored engineering of nucleotide sequences to generate diverse antigens, offering high versatility, expedited development, and cost-effective large-scale production.[1] Furthermore, proteins synthesized from mRNA function as endogenous antigens within the cytoplasm, where they are degraded by the proteasome. The resulting peptides are transported to the endoplasmic reticulum, where they bind to major histocompatibility complex class I molecules and are subsequently presented on the cell surface. Consequently, mRNA-based vaccines effectively present antigens *via* the major histocompatibility complex class I pathway to CD8+ T cells, thereby strongly inducing cellular immunity.[2] This mechanism has been reported to elicit potent antitumor effects, and its application to currently intractable diseases is highly anticipated.[3] Despite these advantages, mRNA therapeutics are currently administered primarily *via* injection, which presents challenges such as severe inflammatory responses at the injection site and pain upon administration. Additionally, injectable administration requires healthcare professionals, which becomes a particularly critical issue during pandemics caused by emerging infectious diseases. Limited access to healthcare professionals and medical infrastructure in developing countries may contribute to delays in vaccination, potentially exacerbating pandemic spread. Moreover, mRNA is an inherently unstable molecule, necessitating low-temperature conditions for long-term storage. This requirement imposes significant logistical and storage challenges, particularly in settings where refrigeration facilities are inadequate. Given these limitations, there is an urgent need to develop a non-invasive and user-friendly alternative to injectable mRNA administration.

[a]*Department of Applied Chemistry, Graduate School of Engineering, Kyushu University, 744 Motooka, Fukuoka 819-0395, Japan.*
E-mail: m-goto@mail.cstm.kyushu-u.ac.jp
[b]*Advanced Transdermal Drug Delivery System Center, Kyushu University, Motooka 744, Nishi-ku, Fukuoka 819-0395, Japan*
[c]*Center for Future Chemistry, Kyushu University, Motooka 744, Nishi-ku, Fukuoka 819-0395, Japan*

Among various non-invasive drug delivery mechanisms, including the oral, ocular, and nasal routes, our research has particularly focused on transdermal delivery. Transdermal administration is advantageous for biopharmaceuticals that are unstable in the body, as it bypasses first-pass metabolism. Additionally, the skin is rich in immune cells, which facilitates the induction of vaccine responses.[4,5] One of the fundamental challenges in transdermal biopharmaceutical delivery, however, lies in the barrier function of the skin. The stratum corneum (SC), the outermost layer of the skin, consists of corneocytes embedded in a highly ordered lipid lamellar structure, functioning as a physical barrier that prevents the penetration of external substances. This barrier limits the permeation of hydrophilic and high-molecular-weight compounds exceeding 500 Da.[11] mRNA is hydrophilic and significantly exceeds 500 Da, thereby limiting its transdermal delivery into the body. Several methods for mRNA transdermal delivery have been investigated, including microneedle technology,[6,7] iontophoresis,[8] and jet injection.[9] For example, Phua *et al.*[10] reported that polymeric microneedles loaded with mRNA successfully delivered mRNA into the skin, enabling protein expression for up to 72 hours. However, these methods require specialized devices, do not ensure complete non-invasiveness, and necessitate administration by healthcare professionals. Therefore, to date, these approaches have not adequately addressed the challenges associated with mRNA vaccine administration.

In recent years, ionic liquids (ILs) have garnered attention as a novel strategy of transdermal drug delivery. ILs are generally defined as salts composed of organic cations and anions that melt below 100 °C.[12] ILs alter the lipid lamellar structure of the SC and enhance intercellular lipid fluidity, thereby increasing transdermal absorption of various drugs. Our research group reported in 2020 the synthesis of ILs using choline (Cho) as the cation and various fatty acids (C10–C18) as anions. These [Cho][Fatty Acid (FA)]-based ILs exhibited low cytotoxicity and improved transdermal permeability of peptide drugs.[13] Furthermore, we developed several nanocarriers based on amphiphilic ILs, achieving transdermal delivery of biomacromolecules such as insulin and ovalbumin.[14,15] In 2023, we successfully synthesized ILs using 1,2-dimyristoyl-*sn*-glycero-3-ethylphosphatidylcholine (EDMPC) as the cation and three types of C18 fatty acids as anions, demonstrating effective transdermal delivery of antisense oligonucleotides.[16] Thus, IL-based carriers hold potential as novel transdermal drug delivery systems (TDDSs) capable of delivering biomacromolecules, particularly nucleic acid therapeutics.

In this study, we focused on lyotropic liquid crystals (LLCs)[17,18] as TDDS carriers. LLCs have been reported to exhibit high affinity for the SC and superior capability in delivering active pharmaceutical ingredients into deeper layers of the skin.[19] LLCs are thermodynamically stable nanostructures composed of amphiphilic molecules in appropriate solvents under specific concentration, temperature, and pressure conditions. This technology has been demonstrated to enhance skin penetration of peptides, antigenic proteins, and siRNA.[17,20–22] Additionally, LLCs form highly ordered, large-scale three-dimensional molecular assemblies, which confer gel-like rheological properties.[23] This characteristic enables LLCs to function as semi-solid formulations, such as ointments or creams, which can be retained on the skin surface, making them an ideal material for TDDSs.

In this study, we developed an efficient transdermal mRNA delivery system using an ionic liquid crystal (ILC), which is an amphiphilic IL-based LLC. The ILC system enables skin permeability from both IL and LLC perspectives while facilitating standardized dosing and improved retention of formulations on the skin. We synthesized ILs ([Cho][Pal], [Cho][Ole]) using Cho, a highly biocompatible cation, and either palmitic acid (Pal) or oleic acid (Ole) anions, demonstrating enhanced skin permeability effects. Then, an ILC was prepared by mixing equal amounts of these ILs to form [Cho][Pal–Ole]. Small-angle X-ray scattering (SAXS) measurements and rheological measurements confirmed the formation of the ILC in each composition. Additionally, mRNA stability tests under conditions containing fetal bovine serum (FBS) suggested that the ILC formed by [Cho][Pal–Ole] has an mRNA protective effect. Furthermore, analysis of the skin penetration mechanism *via* Fourier transform infrared (FT-IR) suggested that [Cho][Pal–Ole] affects the fluidity of SC lipids. Finally, *in vivo* testing using a tumor-bearing mouse model exhibited high preventive antitumor efficacy, suggesting transdermal delivery of mRNA encoding a tumor-associated antigen. Collectively, these results indicate that ILCs using amphiphilic ILs show potential as a novel TDDS platform for mRNA vaccines.

Materials and methods

Materials

Sodium bicarbonate and G418 disulfate were purchased from Sigma-Aldrich (St Louis, MO, USA). Oleic acid (Ole) was obtained from Tokyo Chemical Industry Co., Ltd (Tokyo, Japan). Proteinase K and palmitic acid (Pal) were purchased from FUJIFILM Wako Pure Chemical Corporation (Kyoto, Japan). Ethanol (99%) was obtained from Kishida Chemical Co., Ltd (Osaka, Japan). 2-Mercaptoethanol, sodium pyruvate, Hank's balanced salt solution (HBSS), antibiotic–antimycotic solution, TRIzol®, trypsin–EDTA, and fetal bovine serum (FBS) were purchased from Thermo Fisher Scientific (Waltham, MA, USA). Antibody polymer conjugate (APC) anti-mouse CD8a antibody was obtained from BioLegend (San Diego, CA, USA). Frozen Yucatan micropig (YMP) skin samples were provided by Charles River Laboratories Japan, Inc. (Kanagawa, Japan). Murine skin samples (Hos: HR-1) were purchased from Hoshino Laboratory Animals, Inc. (Ibaraki, Japan). C57BL/6N mice were obtained from Kyushu Animal Experiment Center (Saga, Japan). Optimal cutting temperature (OCT) compound was purchased from Sakura Finetek Japan Co., Ltd (Tokyo, Japan). The PrimeScript RT reagent kit was obtained from Takara Bio Inc. (Shiga, Japan). TruStain FcX™ (anti-mouse CD16/32) was purchased from BD Biosciences (Franklin Lakes,

NJ, USA). PowerUp SYBR Green Master Mix was obtained from Thermo Fisher Scientific.

Animals

All animal experiments were conducted in accordance with the Guidelines for the Care and Use of Laboratory Animals established by the Science Council of Japan, following approval by the Kyushu University Animal Experimentation Committee (Approval No. A24-390-0).

Preparation of mRNA

The NanoLuc-pDNA vector was linearized according to the IVTpro™ mRNA Synthesis System protocol (Takara Bio Inc.). Unless otherwise specified, mRNA encoding NanoLuc was used for experiments. For antitumor efficacy studies, however, mRNA encoding the model tumor antigen peptide $OVA_{257-264}$(SIINFEKL) (molecular weight: 963.13 Da) was employed. This peptide elicits OVA-specific vaccine responses after being delivered to skin dendritic cell subsets, including Langerhans cells and dermal dendritic cells.

Synthesis of ILs

Oleic acid (Ole) and palmitic acid (Pal) were used as organic anions, while choline (Cho) was employed as the cation. The ionic liquids [Cho][Ole] and [Cho][Pal] were synthesized *via* ion-exchange reactions at room temperature, as previously described.[24,25] Briefly, equimolar amounts of sodium bicarbonate choline and the respective fatty acid were added dropwise to methanol and stirred overnight. The solvent was then completely removed using a rotary evaporator, followed by freeze-drying (FD5N, EYELA Tokyo Rika Kikai Co., Ltd, Tokyo, Japan). The synthesized ILs were characterized by ^{1}H NMR spectroscopy (Fig. S1 and S2) and subsequently used for ILC preparation.

Preparation of ILCs

ILCs were prepared by mixing [Cho][Pal] and [Cho][Ole] as the IL components, or by combining [Cho][Pal] and [Cho][Ole] in an equal weight ratio to form [Cho][Pal–Ole] (Fig. 1a), followed by dispersion in ultrapure water. Specifically, the ILs and ultrapure water were mixed at weight ratios of 70 : 30, 50 : 50, and 30 : 70, and the mixtures were centrifuged at 5000*g* for 90 minutes, followed by incubation at 37 °C overnight to obtain the ILCs[26] (Fig. 1b). ILCs encapsulating mRNA as an active pharmaceutical ingredient were prepared by dissolving mRNA in the ultrapure water phase during ILC formulation.

Characterization of ILCs

The prepared ILCs were characterized using small-angle X-ray scattering (SAXS) and a rheometer. For SAXS measurements, ILC samples were placed between sample support films (Rigaku, Tokyo, Japan) and exposed to X-rays for 30 minutes to obtain diffraction patterns. The patterns were acquired using a Nanoviewer system (Rigaku) equipped with a sealed copper tube (Cu-Kα, λ = 0.15418 nm) operating at 40 kV and 30 mA. The sample-to-detector distance was set at 725 mm. The obtained

Fig. 1 Design of the ionic liquid crystal (ILC) system. (a) Structural formula of ionic liquids (ILs). (b) ILC preparation scheme.

images were analyzed using DP2 software (Rigaku), and the scattering vector (q) was calculated using the following equation:

$$q = \frac{4\pi \sin\theta}{\lambda}, d = \frac{2\pi}{q}.$$

For rheological measurements, the ILCs were placed in disposable dishes (Anton Paar, Graz, Austria) and analyzed using a rheometer (MCR501, Anton Paar) equipped with a 25 mm cone-plate system. The angular frequency varied from 0.1 to 500 rad s^{-1}, and data were recorded using a gradient approach.

In vitro skin permeation study

Skin permeation was evaluated using Franz diffusion cells at 32.5 °C, as previously reported.[32] Mouse skin was cut into 2 × 2 cm sections and mounted between the donor and receptor chambers of the Franz diffusion cell. The receptor chamber was filled with 5 mL of phosphate-buffered saline (PBS), while the donor chamber was loaded with 150 μL of PBS or 150 mg of different ILC formulations containing 15 μg of mRNA encoding Nanoluc and incubated at 32.5 °C. After 6 hours, the skin sections were washed with PBS and fixed in OCT compound. The fixed skin was then cryosectioned into 20 μm slices using a cryostat microtome (Leica CM1860UV, Leica Biosystems, Wetzlar, Germany). The skin sections were placed on glass slides and examined for Alexa Fluor® 488-labeled mRNA fluorescence using a confocal laser scanning microscope (CLSM, LSM700 microscope, Carl Zeiss, Oberkochen, Germany). The acquired images were analyzed using LSM software (Carl Zeiss).

Subsequently, mRNA quantification in the mouse skin was performed using the following procedure. The skin sections were washed with PBS and mechanically disrupted using a multi-bead shaker (MB2200, Yasuikikai, Osaka, Japan) equipped with metal beads in a 3 mL disruption tube. TRIzol® was added, and the mixture was vortexed, followed by the addition of chloroform and centrifugation at 16 000*g*, 4 °C, for 15 minutes to isolate RNA. The extracted RNA was purified by

washing with isopropyl alcohol and 70% ethanol, then dissolved in nuclease-free water. The total RNA was subjected to reverse transcription, yielding complementary DNA (cDNA). The relative mRNA levels were quantified using quantitative PCR (qPCR) with a StepOne Real-Time PCR System (Thermo Fisher Scientific, Life Technologies, USA) and PowerUp SYBR Green Master Mix (Thermo Fisher Scientific). For this analysis, NanoLuc For (5′-ACGCCTGATTAATCCGGATGGTAG-3′) and NanoLuc Rev (5′-AGAATACGTTCACACAGACGCCAACC-3′) primers were used.

Evaluation of RNase resistance

Fetal bovine serum (FBS) is known to contain RNase.[27–29] To evaluate the stability of mRNA within the ILCs, we conducted an RNase resistance assay using FBS-containing medium. Specifically, 200 mg of each ILC was incubated with 10% FBS in minimum essential medium (MEM) at 37 °C for 1 hour. Subsequently, 0.2 mg of proteinase K was added and incubated for an additional 1 hour to inactivate RNases. Following incubation, 800 μL of 99% ethanol was added, and the mixture was passed through an EconoSpin™ column (Ajinomoto, Tokyo, Japan). The column was then washed twice with 700 μL of 99% ethanol. The total RNA was extracted and reverse-transcribed into cDNA, and the relative mRNA quantity was determined by real-time PCR using a StepOne Real-Time PCR System (Thermo Fisher Scientific), with Ct values as the output.

FT-IR measurement of SC sheet

SC sheets were prepared according to previously reported methods.[30,31] Briefly, frozen YMP skin was thawed at room temperature, and the epidermal layer was separated from the entire skin by heating the surface to 60 °C using an aluminum incubator. The isolated epidermal sheet was then immersed in trypsin–EDTA for 24 hours to digest the epidermis. The obtained SC sheets were washed with distilled water, dried for 24 hours, and cut into 0.5 × 0.5 cm sections for FT-IR analysis. To evaluate the effect of ILs on the SC sheets, IL was applied to the sheets and incubated at 60 °C for 1 hour. The sheets were then washed with 20% ethanol, thoroughly dried, and subjected to FT-IR analysis. FT-IR measurements were performed using a Spectrum Two spectrometer (PerkinElmer, Waltham, MA, USA). The measurement conditions were set at a resolution of 0.25 cm^{-1}, and each spectrum was obtained by averaging 100 scans. The peak detection function of the FT-IR instrument was used to identify peaks corresponding to symmetric ($symCH_2$) and asymmetric ($asymCH_2$) vibrational modes of lipid alkyl chains.

In vivo tumor experiment

To evaluate the prophylactic antitumor efficacy of ILCs encapsulating mRNA encoding $OVA_{257–264}$(SIINFEKL), cancer cells were transplanted into C57BL/6N mice that had received either subcutaneous injection or transdermal administration of the formulations (Fig. 6a). Specifically, C57BL/6N mice were administered 100 mg of ILC_{30} containing 20 μg of mRNA or 100 μL of PBS *via* transdermal application 14 and 7 days prior to tumor transplantation. As a control, 100 μL of the previously reported lipid nanoparticle (LNP) solution (LipidLaunch™ LNP-102 Exploration Kit, Cayman Chemical Company, Michigan, USA) was subcutaneously injected.

The murine lymphoma cell line E.G7-OVA was used as a tumor model and cultured under the following conditions. The culture medium consisted of RPMI-1640 supplemented with 10% heat-inactivated FBS, 1% antibiotic/antifungal solution, 0.05 mM 2-mercaptoethanol, 1 mM sodium pyruvate, and 400 μg mL^{-1} G418. E.G7-OVA cells were cultured in a 5% CO_2 incubator at 37 °C in 10 cm tissue culture-treated Petri dishes. Prior to transplantation, the cells were stained with trypan blue, counted using a TC20™ Automated Cell Counter (Bio-Rad, Hercules, CA, USA), and resuspended in HBSS (−) at a concentration of 1.0×10^7 cells per mL. Subsequently, E.G7-OVA cells were intradermally injected into the dorsal region of C57BL/6N mice, and tumor growth was monitored for 20 days.

Additionally, at 14 days post-transplantation, tumors were excised, and CD8+ T cells infiltrating the tumor were analyzed using CLSM. Tumor volume was measured every other day from day 1 until day 21 after tumor inoculation by determining the major and minor diameters, and employing the following formula:

$$\text{Tumor volume}\,[\text{mm}^3] = (\text{major axis}\,[\text{mm}]) \times (\text{minor axis}\,[\text{mm}])^2 \times 0.5.$$

If the major axis of the tumor exceeded 20 mm or if ulceration was observed, the mouse was considered to have reached the humane endpoint and was euthanized.

Fourteen days after tumor cell inoculation, the mice were euthanized, and the tumors were excised. The central region of each tumor was dissected, embedded in OCT compound, and sectioned into 20 μm-thick slices on glass slides. After drying, the tumor sections were fixed by immersion in cold acetone for 10 minutes. The sections were then washed with PBS and blocked with Trustain FcX™ to prevent nonspecific antibody binding. After an additional PBS wash, the sections were incubated overnight in a humidified chamber with APC-anti-mouse CD8a antibody. Following incubation, the sections were washed with PBS, and the fluorescence of APC was observed using CLSM.

Statistical analysis

Statistical analysis was performed using Python. The data on skin permeability and tumor volume were tested using Welch's *t*-test, and the data on membrane fluidity were tested using one-way ANOVA. Significance is indicated as * $p < 0.05$, ** $p < 0.01$, and *** $p < 0.001$. Data are expressed as the mean ± standard error (SE) unless specified.

Results and discussion

Preparation and characterization of ILCs

IL was synthesized by an ion exchange reaction between cationic choline (Cho) and anionic fatty acids with carbon chain

lengths of 16 and 18 (Pal and Ole), following a previously reported method.[24] ILC formulations were prepared using [Cho][Pal] only, [Cho][Ole] only, and equal volumes of [Cho][Pal] and [Cho][Ole] at specified concentrations mixed with ultrapure water. Unless otherwise noted, the weight ratio of IL in each formulation is indicated by subscripts. All ILC formulations maintained homogeneity, with no phase separation or precipitation observed. The crystal structure of the ILCs was analyzed by SAXS (Fig. 2). $[Cho][Pal]_{50}$ and $[Cho][Ole]_{30}$ were confirmed to form hexagonal structures because the diffraction peaks showed a ratio of 1, $\sqrt{3}$, 2. This suggests that liquid crystal structures can form even when amphiphilic molecules are used as intercalating layers. Furthermore, for [Cho][Pal–Ole], the diffraction peaks of ILC_{30} showed a ratio of 1, $\sqrt{3}$, 2, and ILC_{50} exhibited a pattern of 1, $\sqrt{3}$. By contrast, ILC_{70} exhibited diffraction peaks with a ratio of $\sqrt{2}$, $\sqrt{3}$. These results suggest that while ILC_{30} and ILC_{50} form hexagonal structures, ILC_{70} adopts a cubic ($Pn3m$) structure.[33] To further evaluate this system, ILCs of [Cho][Pal–Ole] loaded with mRNA were prepared. Comparing the diffraction patterns of mRNA-loaded ILCs with those of drug-free ILCs revealed identical peak patterns, confirming that the presence of mRNA does not alter the crystal structure of ILCs (Fig. S3).

The distribution of [Cho][Pal] and [Cho][Ole] within the ILCs was assessed using fluorescence recovery after photobleaching (FRAP). Specifically, Nile red was used as a fluorescent probe to evaluate the diffusion behavior of the [Cho][Pal–Ole]-containing ILCs (Fig. S4). The results showed a fluorescence recovery rate approaching 100% over time, whereas in ILCs composed solely of [Cho][Pal], the recovery rate remained at approximately 80%. These findings indicate that [Cho][Pal] and [Cho][Ole] are mobile within the ILC, suggesting a homogeneous distribution rather than local domain formation.

Rheological properties are critical factors in determining the applicability of formulations. If the viscoelasticity is too low, the formulation cannot be retained on the skin surface. Therefore, we measured the complex viscosity (η^*), storage modulus (G'), and loss modulus (G'') of ILCs while varying the angular frequency from 0.5 to 500 rad s^{-1}. All ILCs exhibited higher η^* than 8% hydroxyethyl cellulose gel across all frequency points, suggesting the formation of a three-dimensional network structure (Fig. S5a). Furthermore, shear-thinning behavior was observed in the high angular frequency

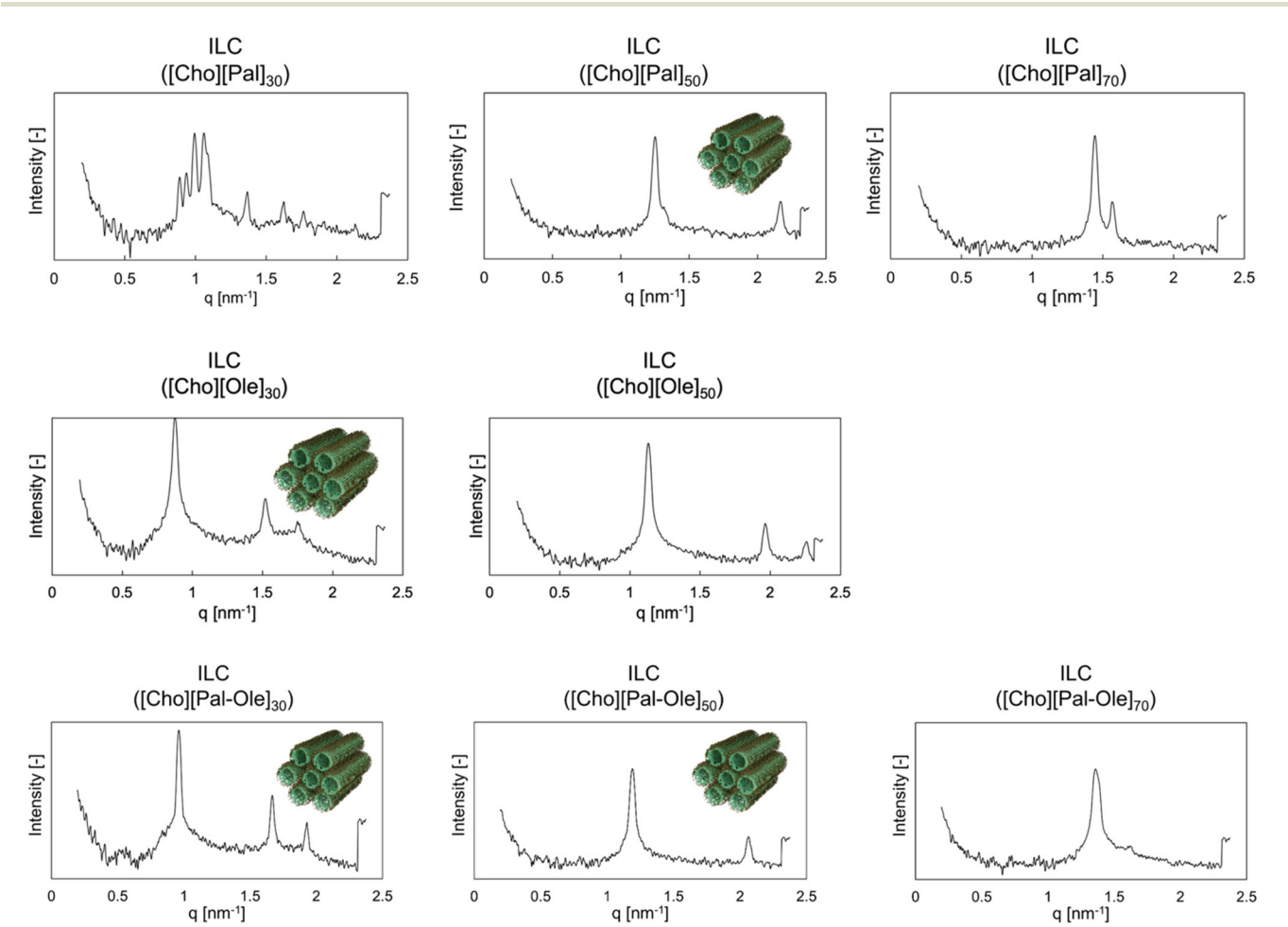

Fig. 2 Small-angle X-ray scattering (SAXS) diffraction pattern of the ILCs.

range, where η^* decreased with increasing frequency. The high viscoelasticity in the low-frequency region indicates that the formulation can be retained on specific skin areas, while the decrease in viscoelasticity at high frequencies indicates that the formulation spreads easily. Additionally, the relationship between G' and G'' is summarized in Fig. S5b. In all samples, G' was dominant over G'', confirming that ILCs exhibit gel-like properties. These results indicate that ILCs possess rheological characteristics suitable for transdermal formulations, making them ideal candidates for TDDSs. We also evaluated the storage stability of mRNA within the ILC formulation (Fig. S6).

In vitro skin permeation

To evaluate the skin permeability of mRNA by ILCs, we used hairless mouse skin as an *in vitro* animal skin model. The skin samples were treated with either PBS containing mRNA labeled with Alexa Fluor 488 or with ILCs. To quantitatively assess mRNA permeation, total RNA was extracted from mouse skin treated with various ILC formulations, and the relative amount of mRNA was determined *via* qPCR, using the PBS-treated group as a reference. The skin permeability of ILCs prepared by [Cho][Pal] is shown in Fig. 3a. Solid-in-oil (S/O) dispersion using [EDMPC][Pal] IL (IL-S/O)[16] was used as a control. The results confirmed that $[Cho][Pal]_{50}$ exhibited higher skin permeability than IL-S/O. Next, we compared the skin permeability of ILCs prepared using $[Cho][Pal–Ole]_{30}$ and [Cho][Ole] (Fig. 3b). The results showed that $[Cho][Pal–Ole]_{30}$ exhibited significantly higher skin permeability than the ILC prepared with [Cho][Ole]. Furthermore, when comparing ILCs and IL-S/O prepared with varying ratios of [Cho][Pal–Ole] (Fig. 3c), $[Cho][Pal–Ole]_{30}$ again demonstrated the highest skin permeability. Finally, the skin permeability of $[Cho][Pal]_{50}$ and $[Cho][Pal–Ole]_{30}$, both exhibiting good skin permeability, was compared (Fig. 3d). Although no significant difference was observed, $[Cho][Pal–Ole]_{30}$ showed higher skin permeability. These findings indicate that $[Cho][Pal–Ole]_{30}$ (ILC_{30}) enhances the transdermal permeation of mRNA. Next, the distribution of mRNA within the skin was examined using CLSM (Fig. 3e). In the PBS-treated group, mRNA was not detected in the deeper layers of the skin, indicating a lack of penetration. By contrast, fluorescence signals were observed in $[Cho][Pal–Ole]_{30}$-treated samples, confirming that mRNA had penetrated beyond the SC into deeper skin layers. Based on these results, ILC_{30} was selected for further studies as it exhibited the highest skin permeability. In subsequent discussions, only [Cho][Pal–Ole], which exhibited the highest permeability, will be referred to. Unless otherwise specified, ILC refers to liquid crystal formulations prepared using [Cho][Pal–Ole].

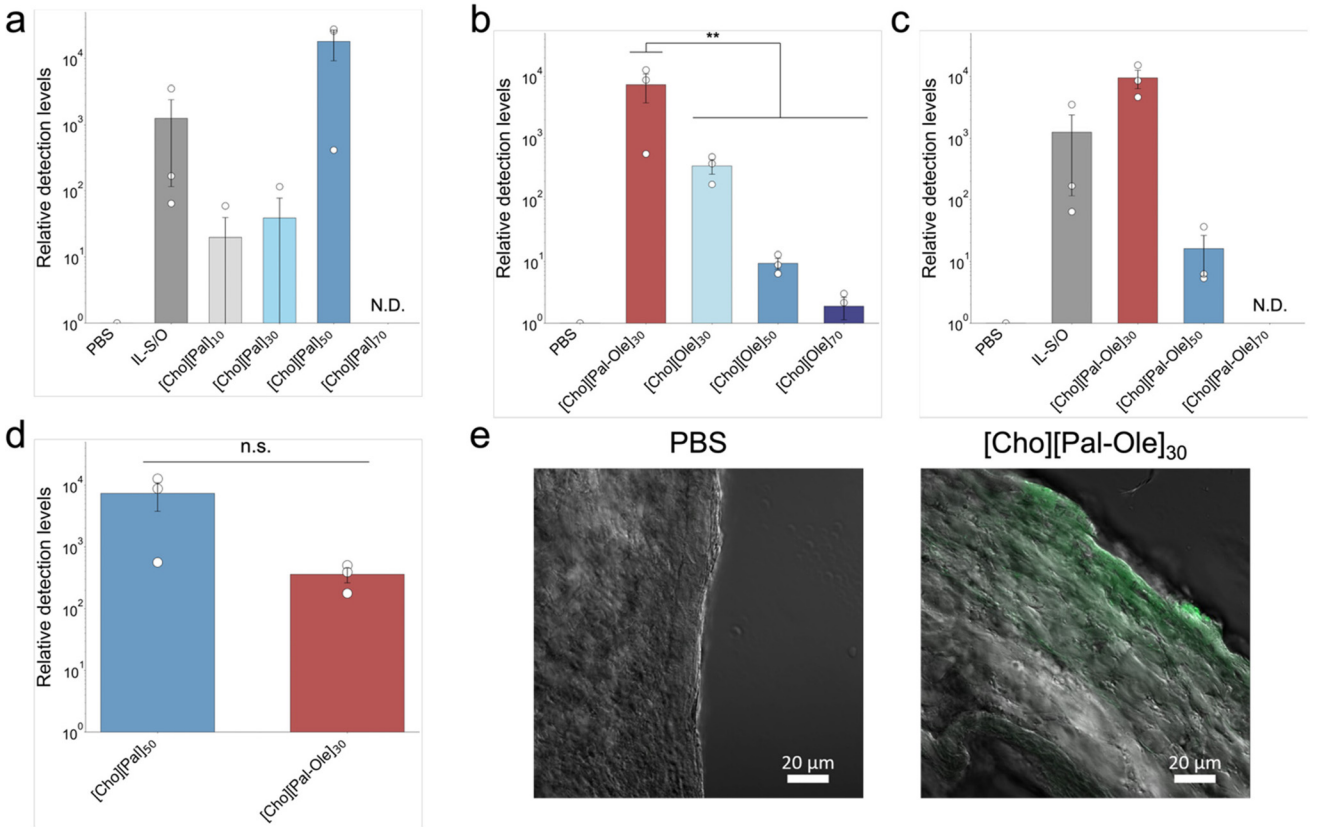

Fig. 3 Skin permeability of mRNA encoding NanoLuc. (a–d) Amount of mRNA that permeated into the mouse skin. (e) CLSM images of cross sections of mouse skin treated with Alexa Fluor® 488-labeled mRNA in PBS or ILC_{30} (mRNA = 10 μg per 100 mg). Images were obtained with a 20× lens. Scale bars: 20 μm. $N = 3$; mean ± SE; $^*p < 0.05$.

Evaluation of mRNA stability in ILCs

mRNA is generally unstable in physical, chemical, and enzymatic environments and is easily degraded. Therefore, we evaluated the protective effect of ILCs on mRNA against RNase degradation. Specifically, ILCs were exposed to 10% FBS/MEM, followed by proteinase K treatment to inactivate proteins. The mRNA was then reverse transcribed into cDNA and quantified *via* qPCR (Fig. 4). The naked mRNA exhibited a significant increase in Ct value, indicating degradation by RNase. By contrast, all ILC formulations showed significantly lower Ct values compared with those for naked mRNA, suggesting that ILCs confer RNase resistance. Furthermore, ILC formulations that were not exposed to 10% FBS/MEM exhibited Ct values comparable to those of ILC formulations exposed to RNase, further confirming the RNase resistance of ILCs.

Evaluation of drug permeation based on chemical changes in the SC

The effect of ILCs on the fluctuation of intercellular lipids was evaluated, and the mechanism by which mRNA passes through the SC was discussed using FT-IR spectroscopy. The FT-IR spectrum of the SC provides crucial information for assessing its structural integrity. Peaks corresponding to the symmetric ($symCH_2$) and asymmetric ($asymCH_2$) stretching vibrations of lipid alkyl chains are observed around 2920 cm^{-1} and 2850 cm^{-1}, respectively. It is known that increased lipid fluctuation in the SC causes a shift toward higher wavenumbers (blue shift) in these peaks.[34] This shift is attributed to a conformational change in the alkyl chains from a fully extended anti-form to a bent *gauche*-form.[35,36] To investigate this phenomenon, SC sheets were isolated from pig skin and treated with three different ILCs for 2 hours. As a result, a blue shift was observed in the peaks near 2920 cm^{-1} and 2850 cm^{-1} upon treatment with ILC_{30} (Fig. 5a and b). This suggests that ILC_{30} disrupts the lipid packing in the SC, thereby facilitating the delivery of high-molecular-weight drugs such as mRNA into deeper layers of the skin.

By contrast, a red shift in the 2920 cm^{-1} and 2850 cm^{-1} peaks was observed with ILC_{50} and ILC_{70}. The insertion of saturated fatty acids into SC lipid packing leads to a red shift.[37] Therefore, a similar phenomenon is considered to have occurred in the ILC_{50} and ILC_{70} formulations.

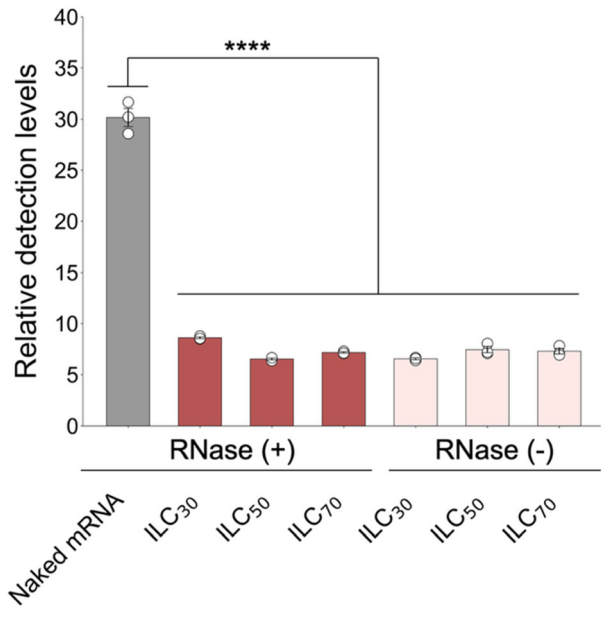

Fig. 4 Cycle threshold (Ct) value in each sample after treatment with RNase. The number of PCR cycles in which the fluorescence signal exceeds a certain threshold is defined as the Ct value. N = 3; mean ± SD; *p < 0.05, ****p < 0.001, n.s. = non significance.

Antitumor efficacy *in vivo*

The administration schedule and dosage are shown in Fig. 6a. C57BL/6N mice were administered 20 μg of mRNA encoding $OVA_{257-264}$(SIINFEKL) per dose either transdermally or *via* injection on days −14 and −7, inoculated with E.G7-OVA, and tumor volume was monitored from day 0 onward. In the positive control group, in which the LNP was administered *via* subcutaneous injection, no tumor formation was observed. By comparison, the ILC_{30} transdermal administration group exhibited significant tumor growth suppression compared with that in the untreated group (Fig. 6b). These findings indicate that ILC_{30} administration achieved an antitumor effect comparable to that of injected formulations. Furthermore, while CD8+ T cells were undetectable in the tumors of untreated mice, a substantial number of CD8+ T cells were observed in the tumors of ILC_{30}-treated mice (Fig. 6c). To further evaluate the therapeutic antitumor efficacy of ILCs, EG.7-OVA tumor cells were transplanted into mice, followed by either injection or transdermal administration, and tumor growth was monitored for 20 days. The injection group exhibited a reduction in tumor size, while in the ILC-treated group, tumor growth suppression was observed, particularly up to day 14, compared with that in the untreated group (Fig. S7a and S7b). This result suggests that ILC-mediated transdermal mRNA delivery led to antigen peptide translation. Additionally, no significant differences in body weight were observed among the groups, and no apparent side effects were detected following ILC administration (Fig. S7c). To further evaluate local skin safety, we monitored transepidermal water loss (TEWL) following topical administration of the ILC formulation as an indicator of skin barrier disruption (Fig. S8). These results suggest that while the ILC formulation induces temporary skin barrier disruption, the effect is reversible and does not result in sustained barrier damage under the tested conditions. In treatment, T cells may become exhausted due to prolonged exposure to large amounts of antigen. Additionally, the tumor microenvironment secretes cytokines such as IL-10 and TGF-β, creating an immunosuppressive environment. As a result, therapeutic interventions introduced later are likely to be less effective. In contrast, prevention occurs when the immune system is functioning normally, potentially yielding better efficacy compared to treatment.

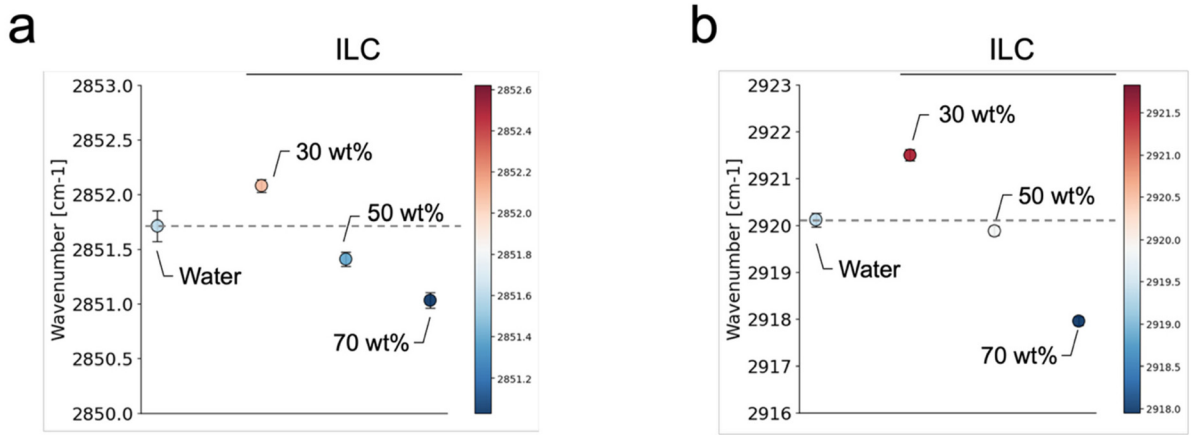

Fig. 5 FT-IR spectra of SC sheets treated with ILC formulations. Peaks at 2850 and 2920 cm^{-1} correspond to CH_2 symmetrical and asymmetrical vibration modes of SC lipids in the intercellular region, respectively.

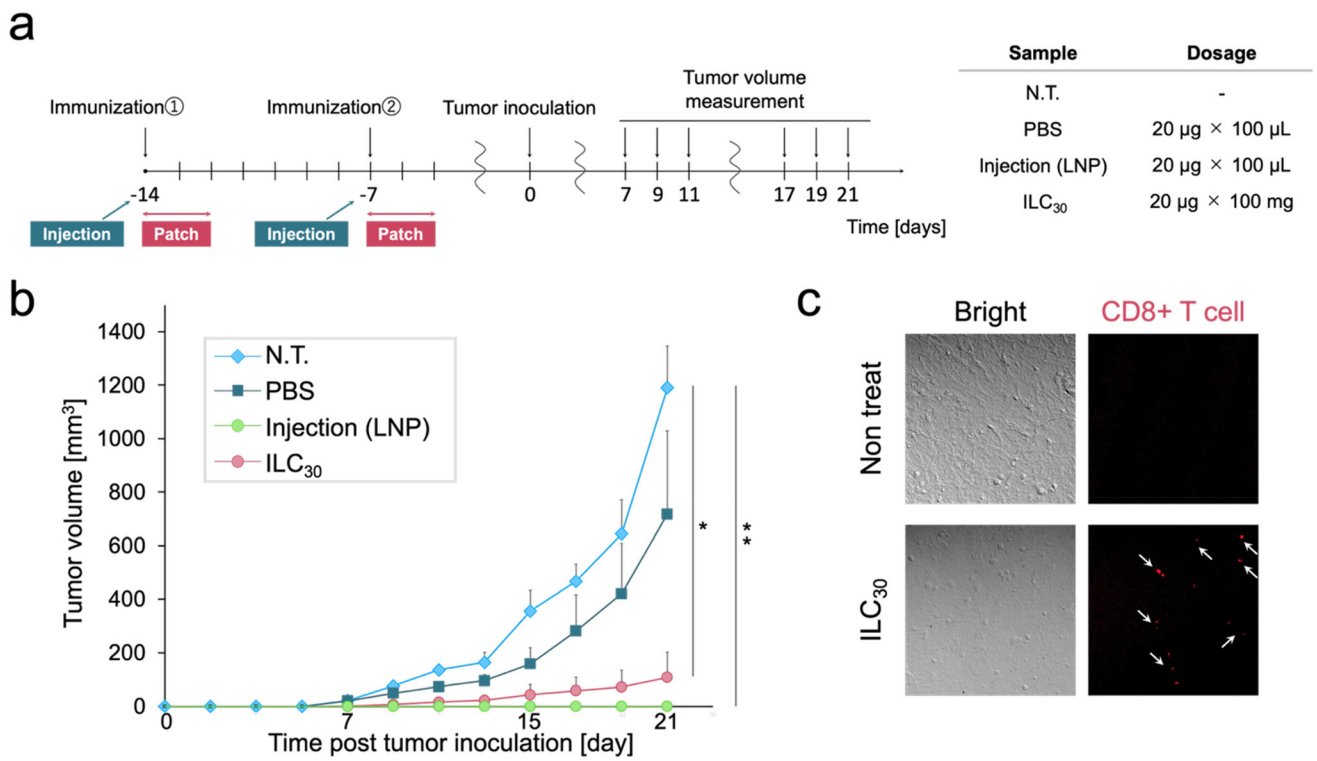

Fig. 6 Prophylactic antitumor effect against E.G7-OVA cells. Prior to tumor inoculation, mRNA encoding $OVA_{257-264}$(SIINFEKL) was administered to C57BL/6N mice by injection and a transdermal patch. The dose of mRNA for each immunization was 20 μg per mouse. (a) Time course of this experiment. (b) Change in tumor volume. (c) Immunohistochemical evaluation of CD8-positive T cells in tumor cross sections at 14 days post-inoculation of E.G7-OVA cells in mice. (Red) APC-labeled anti-CD8 antibody, $N = 4$; mean ± SE; $*p < 0.05$, $**p < 0.01$. Statistical testing was performed on the untreated group and the injection group/ILC group after 21 days.

Conclusions

In this study, we developed a novel ILC formulation for transdermal mRNA delivery using an IL as an amphiphilic molecule. Various ILCs were prepared by altering the weight ratio of ultrapure water to IL, and their physicochemical properties were evaluated. All tested ILCs exhibited suitable rheological properties and RNase resistance, making them promising candidates for transdermal formulations. Notably, among the three types of ILCs examined, ILC_{30} demonstrated the highest skin permeability. This enhanced permeability was attributed to the interaction between ILC_{30} and the intercellular lipids in the SC. Furthermore, *in vivo* evaluation using a tumor-bearing mouse model confirmed the mRNA delivery capability of the

ILC formulation. Compared with tumor growth in the untreated group, the ILC-treated group exhibited significant tumor growth suppression and pronounced infiltration of CD8+ T cells into the tumor tissue. In this study, we used mRNA encoding $OVA_{257-264}$(SIINFEKL) as a model antigen, but this approach is expected to be applicable to other mRNAs encoding different proteins. The ILC-based transdermal delivery system offers significant advantages, including enhanced skin permeability, mRNA stability, and non-invasiveness. However, its formulation complexity may present challenges compared to more established methods like microneedles and iontophoresis. Despite these challenges, the ILC system holds great promise for the non-invasive delivery of mRNA vaccines and other biomacromolecules, paving the way for future advancements in transdermal drug delivery.

Author contributions

T. H.: writing – original draft, investigation, and methodology. K. T., K. T., R. W., Y. K.: investigation and methodology. N. K.: methodology, validation, and writing – review & editing. M. G.: conceptualization, supervision, validation, and writing – review & editing. All authors contributed to the discussion of the paper and approved the manuscript.

Conflicts of interest

There are no conflicts to declare.

Data availability

The data supporting this article have been included as part of the supplementary information (SI). Supplementary information is available. See DOI: https://doi.org/10.1039/d5pm00327j.

Acknowledgements

The authors acknowledge financial support from the Japan Society for the Promotion of Science (KAKENHI number JP22K18314) and from AMED (23ak0101174h0003). We thank Edanz (https://jp.edanz.com/ac) for editing a draft of this manuscript. The authors take responsibility for the final version of the manuscript.

References

1 Y. S. Wang, M. Kumari, G. H. Chen, M. H. Hong, J. P. Y. Yuan, J. L. Tsai and H. C. Wu, *J. Biomed. Sci.*, 2023, **30**, 84.
2 Y. Zhao, D. Boczkowski, S. K. Nair and E. Gilboa, *Blood*, 2003, **102**, 4137–4142.
3 A. L. Coolen, C. Lacroix, P. Mercier-Gouy, E. Delaune, C. Monge, J. Y. Exposito and B. Verrier, *Biomaterials*, 2019, **195**, 23–37.
4 J. C. Joyce, H. E. Sella, H. Jost, M. J. Mistilis, E. S. Esser, P. Pradhan, R. Toy, M. L. Collins, P. A. Rota, K. Roy, I. Skountzou, R. W. Compans, M. S. Oberste, W. C. Weldon, J. J. Norman and M. R. Prausnitz, *J. Controlled Release*, 2019, **304**, 135.
5 N. Romani, M. Thurnher, J. Idoyaga, R. M. Steinman and V. Flacher, *Immunol. Cell Biol.*, 2010, **88**, 424–430.
6 A. vander Straeten, M. Sarmadi, J. L. Daristotle, M. Kanelli, L. H. Tostanoski, J. Collins, A. Pardeshi, J. Han, D. Varshney, B. Eshaghi, J. Garcia, T. A. Forster, G. Li, N. Menon, S. L. Pyon, L. Zhang, C. Jacob-Dolan, O. C. Powers, K. Hall, S. K. Alsaiari, M. Wolf, M. W. Tibbitt, R. Farra, D. H. Barouch, R. Langer and A. Jaklenec, *Nat. Biotechnol.*, 2024, **42**, 510–517.
7 J. Yu, C. Kuwentrai, H. R. Gong, R. Li, B. Zhang, X. Lin, X. Wang, J. D. Huang and C. Xu, *Acta Biomater.*, 2022, **148**, 133–141.
8 M. Hasan, A. Khatun and K. Kogure, *Pharmaceutics*, 2023, **15**, 2678.
9 S. Abbasi, M. Matsui-Masai, F. Yasui, A. Hayashi, T. A. Tockary, Y. Mochida, S. Akinaga, M. Kohara, K. Kataoka and S. Uchida, *Mol. Ther.*, 2024, **32**, 1266–1283.
10 K. J. Koh, Y. Liu, S. H. Lim, X. J. Loh, L. Kang, C. Y. Lim and K. K. L. Phua, *Sci. Rep.*, 2018, **8**, 11842.
11 J. D. Bos and M. M. H. M. Meinardi, *Exp. Dermatol.*, 2000, **9**, 165–169.
12 N. V. Plechkova and K. R. Seddon, *Chem. Soc. Rev.*, 2008, **37**, 123–150.
13 M. Goto, Y. Tahara, K. Morita, R. Wakabayashi and N. Kamiya, *Mol. Pharm.*, 2020, **17**, 3845–3856.
14 F. H. Nabila, R. Islam, I. M. Shimul, M. Moniruzzaman, R. Wakabayashi, N. Kamiya and M. Goto, *Chem. Commun.*, 2024, **60**, 4036–4039.
15 R. Islam, F. H. Nabila, R. Wakabayashi, N. Kamiya, M. Moniruzzaman and M. Goto, *J. Mol. Liq.*, 2024, **397**, 124184.
16 K. Toyofuku, R. Wakabayashi, N. Kamiya and M. Goto, *ACS Appl. Mater. Interfaces*, 2023, **15**, 33299–33308.
17 S. Kozaka, R. Wakabayashi, N. Kamiya and M. Goto, *Acta Biomater.*, 2022, **138**, 273–284.
18 S. Kozaka, R. Wakabayashi, N. Kamiya and M. Goto, *ACS Appl. Mater. Interfaces*, 2021, **13**, 54753–54761.
19 H. Iwai, J. Fukasawa and T. Suzuki, *Int. J. Cosmet. Sci.*, 1998, **20**, 87–102.
20 M. Kawai, H. Ibaraki, Y. Takashima, T. Kanazawa and H. Okada, *Mol. Pharm.*, 2021, **18**, 1038–1047.
21 D. Libster, A. Aserin, E. Wachtel, G. Shoham and N. Garti, *J. Colloid Interface Sci.*, 2007, **308**, 514–524.
22 D. Libster, A. Aserin and N. Garti, *J. Colloid Interface Sci.*, 2011, **356**, 375–386.
23 M. T. Junqueira Garcia, T. Pedralino Gonçalves, É. São Félix Martins, T. Silva Martins, M. Carvalho de Abreu Fantini, P. R. Regazi Minarini, S. Costa Fernandez, G. Cassone

Salata and L. Biagini Lopes, *Int. J. Pharm.*, 2018, **548**, 454–465.
24 M. Goto, Y. Tahara, K. Morita, R. Wakabayashi and N. Kamiya, *Mol. Pharm.*, 2020, **17**, 3845–3856.
25 A. Banerjee, K. Ibsen, Y. Iwao, M. Zakrewsky and S. Mitragotri, *Adv. Healthcare Mater.*, 2017, **6**, 1601411.
26 H. Kim, Z. Song and C. Leal, *Proc. Natl. Acad. Sci. U. S. A.*, 2017, **114**, 10834–10839.
27 N. Yoshinaga, S. Uchida, A. Dirisala, M. Naito, K. Osada, H. Cabral and K. Kataoka, *J. Controlled Release*, 2021, **330**, 317–328.
28 M. Berton, S. Sixou, R. Kravtzoff, C. Dartigues, L. Imbertie, C. Allal and G. Favre, *SupraMolecular BioVector SMBV*, 1997, p. 1355.
29 A. Yen, Y. Cheng, M. Sylvestre, H. H. Gustafson, S. Puri and S. H. Pun, *Mol. Pharm.*, 2018, **15**, 2268–2276.
30 M. Zakrewsky, K. S. Lovejoy, T. L. Kern, T. E. Miller, V. Le, A. Nagy, A. M. Goumas, R. S. Iyer, R. E. DelSesto, A. T. Koppisch, D. T. Fox and S. Mitragotri, *Proc. Natl. Acad. Sci. U. S. A.*, 2014, **111**, 13313–13318.
31 H. Piao, N. Kamiya, A. Hirata, T. Fujii and M. Goto, *Pharm. Res.*, 2008, **25**, 896–901.
32 Y. Tahara, S. Honda, N. Kamiya, H. Piao, A. Hirata, E. Hayakawa, T. Fujii and M. Goto, *J. Controlled Release*, 2008, **131**, 14–18.
33 Y. Huang and S. R. Gui, *RSC Adv.*, 2018, **8**, 6978–6987.
34 A. L. M. Ruela, A. G. Perissinato, M. E. D. S. Lino, P. S. Mudrik and G. R. Pereira, *Braz. J. Pharm. Sci.*, 2016, **52**, 527–544.
35 G. Bernard, M. Auger, J. Soucy and R. Pouliot, *Biochim. Biophys. Acta, Gen. Subj.*, 2007, **1770**, 1317–1323.
36 R. Mendelsohn, C. R. Flach and D. J. Moore, *Biochim. Biophys. Acta, Biomembr.*, 2006, **1758**, 923–933.
37 A. Akinshina, C. Das and M. G. Noro, *Phys. Chem. Chem. Phys.*, 2016, **18**, 17446–17460.